

Nonlinear boundary parameter identification of bridges based on temperature-induced strains

Zuo-Cai Wang^{*1,3}, Guo-Peng Zha¹, Wei-Xin Ren^{1,3}, Ke Hu² and Hao Yang¹

¹Department of Civil Engineering, Hefei University of Technology, Hefei, 230009, Anhui, China

²Anhui Transportation Holding Group Co., Ltd., Hefei, 230088, China

³New Theory and Technology Research Platform of Bridge Structure Safety Monitoring, Hefei University of Technology, Hefei, 230009, China

(Received October 20, 2017, Revised October 9, 2018, Accepted October 23, 2018)

Abstract. Temperature-induced responses, such as strains and displacements, are related to the boundary conditions. Therefore, it is required to determine the boundary conditions to establish a reliable bridge model for temperature-induced responses analysis. Particularly, bridge bearings usually present nonlinear behavior with an increase in load, and the nonlinear boundary conditions cause significant effect on temperature-induced responses. In this paper, the bridge nonlinear boundary conditions were simulated as bilinear translational or rotational springs, and the boundary parameters of the bilinear springs were identified based on the measured temperature-induced responses. First of all, the temperature-induced responses of a simply support beam with nonlinear translational and rotational springs subjected to various temperature loads were analyzed. The simulated temperature-induced strains and displacements were assumed as measured data. To identify the nonlinear translational and rotational boundary parameters of the bridge, the objective function based on the temperature-induced responses is then created, and the nonlinear boundary parameters were further identified by using the nonlinear least squares optimization algorithm. Then, a beam structure with nonlinear translational and rotational springs was simulated as a numerical example, and the nonlinear boundary parameters were identified based on the proposed method. The numerical results show that the proposed method can effectively identify the parameters of the nonlinear boundary conditions. Finally, the boundary parameters of a real arch bridge were identified based on the measured strain data and the proposed method. Since the bearings of the real bridge do not perform nonlinear behavior, only the linear boundary parameters of the bridge model were identified. Based on the bridge model and the identified boundary conditions, the temperature-induced strains were recalculated to compare with the measured strain data. The recalculated temperature-induced strains are in a good agreement with the real measured data.

Keywords: temperature-induced response; boundary condition; parameter identification; model updating; nonlinear least squares optimization

1. Introduction

Temperature-induced responses of bridge structure can cause significant deformation, damage of bearings and local nonlinearities (Dilger *et al.* 1983, Roberts-Wollman *et al.* 2002). Therefore, it is required to determine the temperature-induced responses based on a reliable model. One of the critical issues to establish a reliable model is to identify the bridge model parameters of the bridge boundary conditions, especially when the bearings present nonlinear pattern with the increase of the load.

Previous researches were mainly focused on the temperature distribution analysis and the temperature-induced responses analysis of bridges (Kennedy and Soliman 1987, Shahawy and Arockiasamy 1996, Tong *et al.* 2001). In the last two decades, with the application of bridge health monitoring system, researches on the temperature distribution and temperature-induced responses of bridge structure are increasingly in depth by monitoring

temperature field of bridge section and the measured temperature-induced responses data. For instance, based on the structural temperature monitoring data, Ding *et al.* (2013) obtained the temperature distribution of Runyang Yangtze river bridge, and proposed various temperature models of bridge cross section for temperature-induced responses analysis. By using the temperature monitoring data of many years in Tsing Ma bridge, Xu *et al.* (2009) analyzed the temperature field characteristics of the bridge, on the basis of which the temperature-induced responses are further analyzed. Xia *et al.* (2011) further analyzed the relation between structural vibration characteristics and non-uniform temperature field when the temperature of the structure is non-uniform distribution. Yang *et al.* (2017) investigated the long-term effect of ambient temperature on bridge strain, and a linear regression model between the temperature and the strain due to temperature was established based on one year monitoring data.

However, the temperature-induced responses are not only related to temperature field of the bridge cross section but also the bridge parameters. To determine the temperature-induced responses is required to establish a reliable model. Recently, bridge model updating methods based on vibration data were developed to obtain the bridge

*Corresponding author, Professor
E-mail: wangzuocai@hfut.edu.cn

model parameters (Jaishi and Ren 2005, Ren *et al.* 2005, Brownjohn *et al.* 2011). For instances, Nagayama *et al.* (2005) applied a bridge model parameter identification method to a full-scale suspension bridge. He *et al.* (2009) identified the bridge system parameters of a real bridge based on the dynamic field test data. Zhang *et al.* (2013) used a dynamic data post-processing method to identify the bridge dynamic characteristics based on the experimental vibration test of a long-span suspension bridge. Deng *et al.* (2010) further based on the updated bridge model to assess a long-span suspension bridge using long-term monitoring data. Chen *et al.* (2014) explored a novel damage detection technique based on stress influence lines of bridge components and validated the efficacy of the technique through a case study of the Tsing Ma suspension bridge. Since complex nonlinear behavior of structures has been observed not only when they are subjected to extreme loads, but also during the operational conditions, therefore, nonlinear structural system identification was received wide attentions in recent years. To identify the structural nonlinear parameters, Lei *et al.* (2015) presented an extended Kalman filter based method for structural nonlinear restoring forces identification, and the parameters of structural nonlinear restoring forces at the locations of the structural nonlinearities together with the linear part structural parameters can be identified in the study. Yu and Zhu (2015) proposed an integrated method for structural nonlinear damage detection based on time series analysis and the higher statistical moments of structural responses. Wang *et al.* (2015) quantified the structural nonlinearity based on the time-frequency features of the dynamic responses of the nonlinear structures. In real cases, the nonlinearity of the structure is usually observed in local elements, such as bearings, connections, and so on. Therefore, it is more reliable to detect the local nonlinearity of the structure. Ni *et al.* (2007) evaluated a bridge expansion joints using the long-term displacement and temperature measurements. Alamdari *et al.* (2014) introduced a nonlinear joint model updating method based on structural nonlinear frequency response function. Li *et al.* (2015) detect the damage of the shear connector linked the slab and girder based on the power spectral density transmissibility method. Wang *et al.* (2016) presented a model updating method based on the instantaneous amplitude and frequency of the measured dynamic response for structural joint nonlinear parameter identification. Gao *et al.* (2017) established the restoring force model for the cable-sliding modular expansion joints of continuous beam bridges to control the relative displacement and avoid collision when subjected to ground motions.

Although the vibration based structural nonlinear parameter identification methods are very useful, it is hard to observe the variation of the structural boundary condition over a relative long time scale, especially, when the boundary conditions are changed due to the long term temperature effect or other long term load. As an alternative bridge parameter identification method, temperature induced responses are used for bridge parameter identification. In recent years, bridge parameter identification based on temperature induced response of site

monitoring system has received increasing attention. For instance, Moaveni and Behmanesh (2012) updated the parameters of Dowling Hall pedestrian bridge based on temperature induced responses. Wei and Lv (2015) identified both local damages and the temperature difference in a gradient-based model updating method based on dynamic response sensitivity considering temperature effect. Yarnold and Moon (2015) and Yarnold *et al.* (2015) made comparative studies with bridge parameter identification based on temperature induced responses and vibration responses for Tacony-Palmyra bridge. Their results indicated that the accuracy of the identification methods based on temperature induced responses presents higher precision.

In bridges, the bearings are critical local elements and usually present nonlinear pattern with the long term or extreme loads. Therefore, to establish a reliable model for temperature induced responses analysis, the boundary parameters of the bridge need to be calibrated. Therefore, there is growing recognition that the boundary conditions of the structural model need to be determined for bridge identification. Chaudhary *et al.* (2002) presented a two-stage system identification method for bridge bearing stiffness and damping identification. Their results indicated that the identified bearing stiffness when the bridge is subjected to low-level excitations is larger than the values when the bridge is subjected to the high-level excitations. This phenomenon means the identified bearing stiffness is changed due to the level of excitations and presents nonlinear behavior. Dai *et al.* (2006) analyzed the effect of the stiffness of the rubber pads on the dynamic characteristics of a base-isolated bridge.

In this paper, the relation between the nonlinear boundary conditions and the temperature induced responses were established based on the theoretical derivation of a beam structure with nonlinear translational and rotational boundary conditions. Moreover, the optimal objective function, based on temperature induced strains and displacements, was established for the nonlinear boundary conditions identification of the bridge. The nonlinear boundary parameters were identified by using the nonlinear least squares optimization algorithm. A beam structure with nonlinear translational and rotational boundary conditions was simulated as numerical example. The numerical results show that the bilinear boundary conditions can be effectively identified based on the temperature induced responses. Since the nonlinear boundary conditions can be caused by the dead load, live load and temperature load, therefore, the nonlinear boundary parameters were also identified based on the strain induced by these loads combination. Finally, according to the measured data of a tied arch bridge, the boundary condition parameters of the arch bridge were identified based on the proposed method. Since the bearings of the bridge did not perform nonlinear behavior, only the linear boundary parameters were identified. Based on the bridge finite element model and the identified boundary conditions, the temperature-induced strains were recalculated. The recalculated temperature-induced strains are in a good agreement with the real measured data.

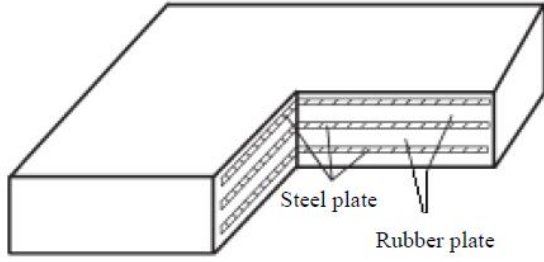


Fig. 1 Steel rubber bearing

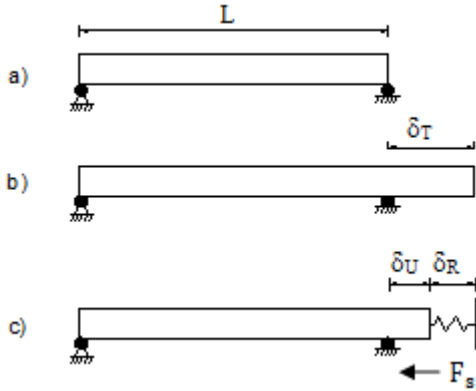


Fig. 2 Deformation diagram of beam structure w/o translational constraint spring under uniform temperature change

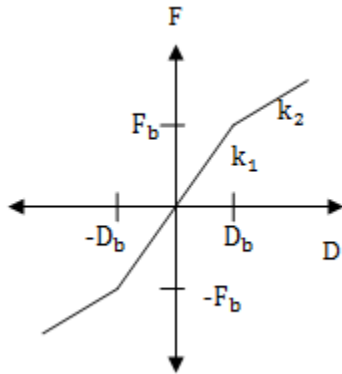


Fig. 3 The constitutive relationship of the force-displacement curve of the bilinear translational spring

2. Temperature induced responses of a beam structure with nonlinear boundary conditions

The fixed hinge rubber bearing and the sliding rubber bearing are the two basic bearings in bridges. A simple steel rubber bearing is presented in Fig. 1. In real cases, the stiffness of the fixed hinge rubber bearing cannot be infinity, and the stiffness of the sliding rubber bearing cannot be zero. Therefore, the bearings are usually simulated as spring elements with translational and rotational rigidities. In this section, a beam structures with bilinear translational and rotational boundary conditions is considered. The temperature induced displacements and strains of beam structure with bilinear translational condition subjected to uniform temperature change, and the

bilinear rotational boundary condition subjected to linear temperature gradients are theoretically derived.

2.1 Temperature induced responses of a beam structure with bilinear translational boundary condition under uniform temperature change

A simple beam without translational constraint spring shows as Fig. 2(a). In the condition of the uniform temperature rise, the deformation of the simple beam shows as Fig. 2(b). In Fig. 2(b), δ_T is the translational deformation without translation constraint. When the translational deformation is constrained by a translational spring, the deformation of the beam structure is presented in Fig. 2(c). In Fig. 2(c), δ_U is the translational deformation with translation constraint, and δ_R is the constrained deformation. If the translation constraint appears to be the bilinear spring constraint, the constitutive relation curve between force and displacement can be presented as Fig. 3. In Fig. 3, F_b and D_b are the transitional load and displacement of the bilinear spring, respectively. k_1 and k_2 are the stiffness of the two stage of the bilinear spring. The expressions of the displacement δ_U and the strain of cross section ε_M of the beam structure with bilinear translation boundary conditions under the action of uniform temperature change can be obtained by the following theoretical derivation.

When $\delta_U < D_b$, the theoretical relationship between displacement δ_U and strain of the cross section ε_M can be calculated as.

$$\delta_U = \frac{\alpha (T - T_0) L}{1 + \frac{k_1 L}{AE}} \quad (1)$$

$$\varepsilon_M = -\frac{k_1 \alpha (T - T_0) L}{AE(1 + \frac{k_1 L}{AE})} \quad (2)$$

where, L is the initial length of the simple beam, α is the coefficient of thermal expansion, A is the cross-sectional area, E is the elastic modulus, T_0 is the initial temperature, T is the global temperature after temperature change, and k_1 is the initial stiffness value of the bilinear translational spring.

When $\delta_U > D_b$, the theoretical relationship between displacement δ_U and strain ε_M can then be calculated as,

$$\delta_U = \frac{F_b}{k_1} + \frac{\alpha (T - T_0) L - \frac{F_b}{k_1} - \frac{F_b L}{AE}}{1 + \frac{k_2 L}{AE}} \quad (3)$$

The relationship between the uniform temperature change and the temperature induced displacement and strain can be calculated as Eq. (4),

$$\varepsilon_M = -\frac{F_b}{AE} - \frac{k_2 \alpha (T - T_0) L - \frac{k_2 F_b}{k_1} - \frac{k_2 F_b L}{AE}}{AE(1 + \frac{k_2 L}{AE})} \quad (4)$$

where, k_2 is the stiffness value of the second stage of the bilinear translational spring, and F_b is the transitional force which is required for the translational boundary condition of the beam reaching the bilinear second stage. If $\delta_U < D_b$, the

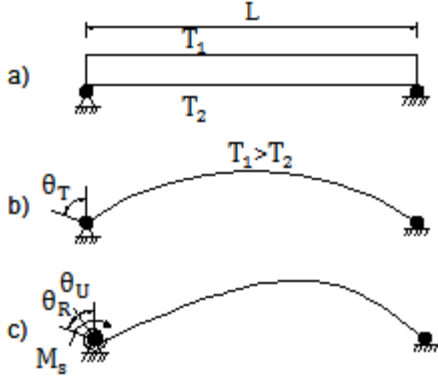


Fig. 4 Deformation diagram of beam structure w/o rotational constraint spring under linear gradient temperature

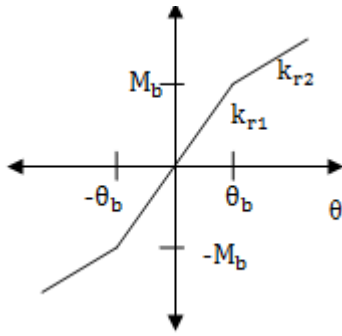


Fig. 5 The constitutive relationship of the moment-rotation curve of the bilinear rotational spring

stiffness of the translational spring remains k_1 , and the uniform temperature change has linear relationship with temperature induced displacement and strain. When $\delta_U > D_b$, the stiffness of the translational spring reduces to k_2 .

2.2 Temperature induced responses of a beam structure with bilinear rotational boundary condition under linear gradient temperature change

A simple beam without rotational constraint spring shows as Fig. 4(a). In the condition of the gradient temperature rise, the deformation of the simple beam shows as Fig. 4(b). The deformation of the beam structure with the rotational constraint boundary condition subjected to gradient temperature is shown in Fig. 4(c). In this paper, the rotational constraint spring is assumed to be bilinear rotational constraint spring, and the constitutive relation curve between moment and rotation is further illustrated in Fig. 5. In Fig. 4, T_1 and T_2 are the temperature on the top surface and bottom surface, respectively. θ_T is the rotational angle of the beam pin end without rotational constraint spring. θ_U is the rotational angle of the beam pin end with rotational constraint spring, and θ_R is the constrained rotational angle. In Fig. 5, M_b and θ_b are the transitional moment and rotational angle of the bilinear rotational constraint spring, respectively. k_{r1} and k_{r2} are the stiffness of the two stage of the bilinear rotational constraint spring. The expressions of the rotational angle θ_U and the strain ε_R of the beam structure with bilinear rotational constraint

spring under the uniform gradient temperature change can be obtained by the following theoretical derivation.

When $\theta_U < \theta_b$, the theoretical relationship between the rotational angular displacement θ_U and the strain ε_M is calculated as,

$$\theta_U = -\frac{\alpha(T_1 - T_2)}{2h(1 + \frac{k_{r1}L}{3EI})} \quad (5)$$

$$\varepsilon_R = -\frac{k_{r1}\alpha(T_1 - T_2)y}{2hEI(1 + \frac{k_{r1}L}{3EI})} \quad (6)$$

where, L is the initial length of the simple beam, α is the coefficient of thermal expansion, h is the height of beam structure, E is the elastic modulus, I is the inertia moment of cross-section, T_1 is the temperature of the top surface, T_2 is the temperature of the bottom surface, and y is the distance to neutral axis. Here, the positive direction of y points down, therefore, at the bottom surface, $y=h/2$, the strain has minus sign which means the stress is compressive strain.

When $\theta_U > \theta_b$, the theoretical relationship between the rotational angular displacement θ_U and the strain ε_R is calculated as.

$$\theta_U = -\frac{M_b}{k_{r1}} - \frac{\alpha(T_1 - T_2)}{2h(1 + \frac{k_{r2}L}{3EI})} + \frac{\frac{M_b}{k_{r1}}(1 + \frac{k_{r1}L}{3EI})}{(1 + \frac{k_{r2}L}{3EI})} \quad (7)$$

$$\varepsilon_R = -\frac{M_b y}{EI} - \frac{k_{r2}\alpha(T_1 - T_2)y}{2hEI(1 + \frac{k_{r2}L}{3EI})} + \frac{k_{r2}\frac{M_b}{k_{r1}}(1 + \frac{k_{r1}L}{3EI})y}{EI(1 + \frac{k_{r2}L}{3EI})} \quad (8)$$

where, k_{r2} is the rotational stiffness value of the second stage of the bilinear rotational constraint spring. M_b and θ_b are the transitional moment and rotational angle of the bilinear rotational constraint spring, respectively.

As presented in Eqs. (7) and (8), when $\theta_U < \theta_b$, the rotational stiffness of the rotational constraint spring remains k_{r1} , and the temperature difference between the top and bottom surfaces has linear relationship with the gradient temperature induced rotation angle and strain. When $\theta_U > \theta_b$, the stiffness of the rotational constraint spring reduces to k_{r2} . The relationship between the temperature difference between the top and bottom surfaces and the gradient temperature induced rotation angle and strain can be calculated as Eq. (8).

2.3 Temperature induced responses of a beam structure

A simulated beam structure with the bilinear translational spring at the beam end is shown in Fig. 6. The main parameters of beam structure are shown in Table 1.

The real stiffness values of the bilinear translational spring are, $k_1=440$ kN/mm, $k_2=40$ kN/mm, and the transitional load, $F_b=530$ kN. A strain sensor is assumed to

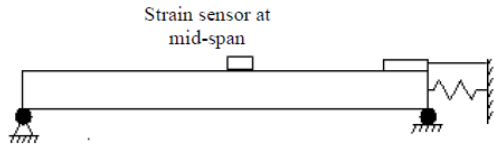


Fig. 6 The simulated beam structure with bilinear translational spring at the beam end

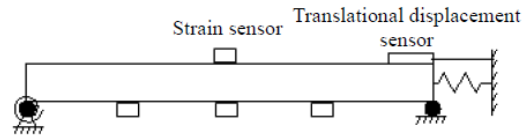


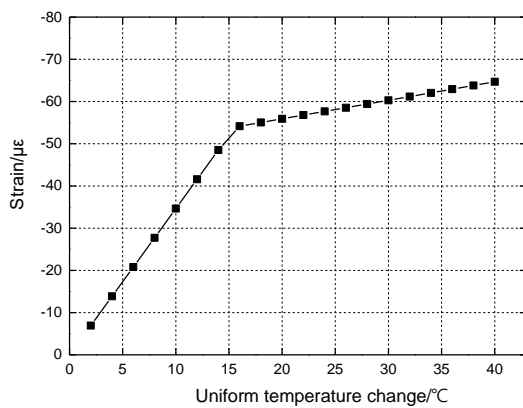
Fig. 8 The simulated beam structure with bilinear translational spring and rotational spring at each end

Table 1 Basic parameters of the beam structure

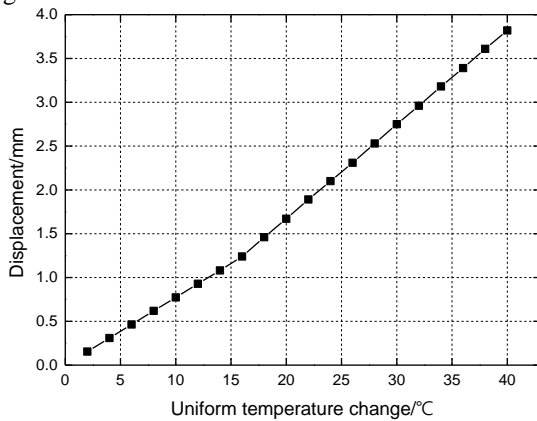
| Beam structure parameter | Real value |
|---|--|
| length of the beam span, L | 10 m |
| elastic modulus, E | 200 GPa |
| area of cross section, A | $4.91 \times 10^{-2} \text{m}^2$ |
| coefficient of thermal expansion α | $1.12 \times 10^{-5} / ^\circ\text{C}$ |

Table 2 The calculated strains and displacements of the beam structure under various temperature load conditions

| Temperature increased on top surface ($^\circ\text{C}$) | Temperature increased on the bottom surface ($^\circ\text{C}$) | Calculated translational displacement (mm) | Strain ($\mu\epsilon$) | | | |
|---|--|--|----------------------------|----------------------------|----------------------------|-------------------------|
| | | | Bottom surface at 1/4-span | Bottom surface at 1/2-span | Bottom surface at 3/4-span | Top surface at 1/2-span |
| 18 | 10 | 1.0 | -12.6 | -11.6 | -10.5 | -7.5 |
| 25 | 15 | 1.6 | -14.8 | -13.6 | -12.4 | -8.7 |
| 30 | 18 | 1.9 | -16.4 | -15.0 | -13.6 | -9.4 |
| 35 | 20 | 2.1 | -17.9 | -16.2 | -14.5 | -9.4 |
| 45 | 25 | 2.7 | -21.0 | -18.8 | -16.7 | -10.2 |



(a) Strain at mid-span under various uniform temperature changes



(b) Displacement at end-span under various uniform temperature changes

Fig. 7 Strain at mid-span and displacement at end-span under various uniform temperature changes

be installed at the top of mid-span, and a translational displacement sensor is assumed to be installed at the end of span. Based on the previous theoretical derivation, the strain at the mid-span and the translational displacement at the end-span due to uniform temperature changes from 0 to 40 $^\circ\text{C}$ with 2 $^\circ\text{C}$ interval are calculated, and the results are presented in Fig. 7. As presented in Fig. 7(a) and Fig. 7(b), at the first stage, the stiffness of the translation spring is

strong, and the displacement at end-span increase relatively slowly, and the strain at mid-span increase relatively fast when the temperature increases. However, at the second stage, the stiffness value of the bilinear translational spring reduces to 40 kN/mm, the displacement at end-span increase relatively fast, and the strain at mid-span increase relatively slowly when the temperature keeps increasing.

In order to further calculate the temperature induced responses in a complex beam structure, a simulated beam structure with a bilinear translational spring and a rotational spring is considered in this case. The simulated beam structure is shown in Fig. 8. The basic parameters of the simulated beam are also shown table. The height of beam is 0.22 m. The real stiffness values of the bilinear translational spring are, $k_1=100$ kN/mm, $k_2=30$ kN/mm, and the real transitional load is, $F_b=89.5$ kN. The real stiffness values of the bilinear rotational spring are, $k_{r1}=3 \times 10^7 \text{N} \times \text{m} / \text{rad}$, $k_{r2}=1 \times 10^7 \text{N} \times \text{m} / \text{rad}$, and the real transitional moment is, $M_b=1089 \text{N} \times \text{m}$. In this case, the strain sensors are assumed installed at the bottom of 1/4-span, mid-span, 3/4-span, and top of mid-span. A translational displacement sensor is assumed to be installed at the end of span with a translational spring. The strains and displacements under various temperature load conditions are presented in Table 2.

3. Nonlinear boundary parameter identification of a beam structure

In this section, the nonlinear boundary parameters of a beam structure are identified based on the measured temperature induced responses. The optimization objective function is then established based on the temperature induced responses. The boundary parameters of bilinear translational and rotational springs are obtained by optimizing the created objective function in various load conditions.

Table 3 The identified boundary parameters of a beam structure with a translational spring

| The identified parameter | Theoretical value | Identified value | Error |
|--------------------------|-------------------|------------------|-------|
| F_b | 530 kN | 539 kN | 2% |
| D_b | 1.2 mm | 1.2 mm | 0% |
| k_1 | 440 kN/mm | 449 kN/mm | 2% |
| k_2 | 40 kN/mm | 42 kN/mm | 5% |

Table 4 The identified boundary parameters of a beam structure with translational and rotational springs

| The identified parameter | Theoretical value | Identified value | Error |
|--------------------------|--------------------------|-----------------------------|-------|
| F_b | 89.5 kN | kN | 1% |
| D_b | 0.9 mm | 0.9 mm | 0% |
| k_1 | 100 kN/mm | 100 kN/mm | 0% |
| k_2 | 30 kN/mm | 30.4 kN/mm | 1% |
| M_b | 1089 N×m | 1000 N×m | -8% |
| θ_b | 3.6×10^{-5} rad | 3.3×10^{-5} rad | -8% |
| k_{r1} | 3×10^4 kN×m/rad | 3.02×10^4 kN×m/rad | 1% |
| k_{r2} | 1×10^4 kN×m/rad | 1.02×10^4 kN×m/rad | 1% |

3.1 Boundary parameter identification of a beam structure with a bilinear translational spring

A beam structure with a bilinear translational spring at the beam end is considered in the section. The beam structural is the same as presented in section 2.3. The basic parameters of the beam are also presented in table 1, and the strain at the top of mid-span and displacement at the end-span are presented in Fig. 6. The simulated strain at the top of mid-span, and the displacement at the end-span under uniform temperature changes from 0 to 40°C with 2°C interval are assumed as measured values.

According to measured temperature induced strains and displacements of the beam structure with bilinear translation boundary conditions, the optimization objective function can be established as.

$$F = \sum_{i=1}^n R_\varepsilon(i)^2 + \sum_{i=1}^n R_d(i)^2 \quad (9)$$

$$R_\varepsilon(i) = \frac{\varepsilon_{measured}(i) - \varepsilon_{theoretical}(i)}{\varepsilon_{theoretical}(i)} \times 100\% \quad (10)$$

$$R_d(i) = \frac{d_{measured}(i) - d_{theoretical}(i)}{d_{theoretical}(i)} \times 100\% \quad (11)$$

in which, R_ε is the normalized error between the measured temperature induced strain $\varepsilon_{measured}$ of the beam structure and the theoretical temperature induced strain $\varepsilon_{theoretical}$, R_d is the normalized error between the measured temperature induced displacement $d_{measured}$ of the beam structure and the theoretical temperature induced displacement $d_{theoretical}$, i is the i^{th} uniform temperature change load case, and n is the total uniform temperature

change load cases, which is equal to 20 in this case.

In this case, $\varepsilon_{theoretical}$ and $d_{theoretical}$ are the function of the bilinear stiffness values of the translational spring k_1 and k_2 , and the transitional load and displacement F_b and D_b . By minimize the objective function of Eq. (9), the boundary parameters can be obtained. In this paper, the Levenberg-Marquardt nonlinear optimization approach (Marquardt 1963) is used to obtain the boundary parameters.

The identified boundary parameters are shown in Table 3. As presented in Table 3, the bilinear stiffness values of the translational spring k_1 and k_2 , and the transitional load and displacement F_b and D_b are well identified. The maximum error of the identified boundary parameter is 5%.

3.2 Boundary parameters identification of a beam structure with bilinear translational and rotational springs

Case 1: In order to further identify the boundary parameters based on the temperature induced responses in a complex beam structure, a beam structure with a bilinear translational spring and a bilinear rotational spring is considered in this case. The beam structural is the same as presented in section 2.3, and the model is presented in Fig.8 in section 2.3. The basic parameters of the beam are presented in Table 1. The strain sensors are assumed installed at the bottom of 1/4-span, mid-span, 3/4-span, and top of mid-span. A translational displacement sensor is assumed to be installed at the end of span with a translational spring. The simulated strains and displacements are presented in Table 2 and assumed as measured data. According to the measured temperature induced strains and displacements of the beam structure with bilinear translation and rotational boundary conditions, the optimization objective function can be established as,

$$F = \sum_{j=1}^m \sum_{i=1}^n R_\varepsilon(i, j)^2 + \sum_{i=1}^n R_d(i)^2 \quad (12)$$

As the same as Eqs. (9) to (11), R_ε is the normalized error between the measured temperature induced strain $\varepsilon_{measured}$ of the beam structure and the theoretical temperature induced strain $\varepsilon_{theoretical}$. R_d is the normalized error between the measured temperature induced displacement $d_{measured}$ of the beam structure and the theoretical temperature induced displacement $d_{theoretical}$. i is the i^{th} temperature load case, and n is the total temperature load cases, which is equal to 5 in this case. j is the j^{th} measured points, and m is the total measure points, which is equal to 4 in this case.

In this case, $\varepsilon_{theoretical}$ and $d_{theoretical}$ are the function of the bilinear stiffness values of the translational spring k_1 and k_2 , the transitional load and displacement F_b and D_b , the bilinear stiffness values of the rotational spring k_{r1} and k_{r2} , and the transitional moment M_b and rotational angle θ_b of the bilinear rotational constraint spring. By minimize the objective function of Eq. (12), the boundary parameters can be obtained. Again, the Levenberg-Marquardt nonlinear optimization approach is also used to obtain the boundary parameters.

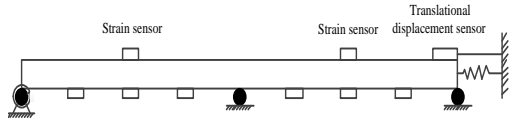


Fig. 9 The simulated continuous beam structure with bilinear translational spring and rotational spring at each end

Table 5 Basic parameters of the continuous beam structure

| Continuous beam structure parameter | Real value |
|---|--------------------------------------|
| length of the beam span, L | 2×10 m |
| elastic modulus, E | 200 GPa |
| area of cross section, A | $4.91 \times 10^{-2} \text{m}^2$ |
| coefficient of thermal expansion α | $1.12 \times 10^{-5}/^\circ\text{C}$ |

Table 6 The calculated strains and displacements of the beam structure under various temperature load conditions

| Temperature increased on | | Translational displacement (mm) | Span 1 Strain ($\mu\epsilon$) | | | Span 2 Strain ($\mu\epsilon$) | | | | |
|----------------------------------|-------------------------------------|---------------------------------|---------------------------------|----------|----------|---------------------------------|----------|----------|----------|-------|
| top surface ($^\circ\text{C}$) | bottom surface ($^\circ\text{C}$) | | Bottom surface at | | | Top surface at | | | | |
| | | | 1/4-span | 1/2-span | 3/4-span | 1/4-span | 1/2-span | 3/4-span | 1/2-span | |
| 18 | 10 | 1.5 | -13.2 | -10.1 | -12.4 | -8.3 | -15.8 | -13.1 | -10.5 | -9.6 |
| 25 | 15 | 2.1 | -16.5 | -12.6 | -12.9 | -10.4 | -19.8 | -16.4 | -13.1 | -12.3 |
| 30 | 18 | 2.5 | -20.1 | -15.2 | -14.4 | -12.5 | -23.8 | -19.7 | -16.2 | -14.3 |
| 35 | 20 | 2.9 | -25.9 | -19.1 | -17.9 | -15.6 | -29.9 | -24.7 | -20.6 | -17.6 |
| 45 | 25 | 3.7 | -35.3 | -25.7 | -22.8 | -20.9 | -40.1 | -33 | -28.1 | -23.3 |

The identified boundary parameters are presented in Table 4. As presented in Table 4, the bilinear stiffness values of the translational spring k_1 and k_2 , and the transitional load and displacement F_b and D_b are well identified. The maximum error of the identified boundary parameter of the translational spring is within 1%. The bilinear stiffness values of the rotational spring k_{r1} and k_{r2} , and the transitional moment M_b and rotational angle θ_b are also well identified, and the error is within 8%.

Case 2: To further verify the effectiveness of the proposed method, a continuous beam structure with a bilinear translational spring and a bilinear rotational spring is considered in this case. The continuous beam structure model is shown in Fig. 9. The basic parameters of the beam are presented in Table 5. The height of the beam is 0.22 m with two spans. The real stiffness values of the bilinear translational spring are, $k_1=100$ kN/mm, $k_2=30$ kN/mm, and the real transitional load is, $F_b=89.5$ kN. The real stiffness values of the bilinear rotational spring are, $k_{r1}=3 \times 10^7$ N×m/rad, $k_{r2}=1 \times 10^7$ N×m/rad, and the real transitional moment is, $M_b=1089$ N×m. In this case, the strain sensors are assumed installed at the bottom of 1/4-span, mid-span, 3/4-span, and top of mid-span of each span. A translational displacement sensor is assumed to be installed at the end of the second span with a translational spring. The strains and displacements under various temperature load conditions are presented in Table 6.

The identified boundary parameters are presented in

Table 7 The identified boundary parameters of a beam structure with translational and rotational springs

| The identified parameter | Theoretical value | Identified value | Error |
|--------------------------|--------------------------|-----------------------------|-------|
| F_b | 89.5 kN | 90.5 kN | 1.1% |
| D_b | 0.9 mm | 0.89 mm | -1.1% |
| k_1 | 100 kN/mm | 101 kN/mm | 1.0% |
| k_2 | 30 kN/mm | 30.7 kN/mm | 2.3% |
| M_b | 1089 N×m | 994 N×m | -8.7% |
| θ_b | 3.6×10^{-5} rad | 3.32×10^{-5} rad | -7.8% |
| k_{r1} | 3×10^4 kN×m/rad | 3.06×10^4 kN×m/rad | 2.0% |
| k_{r2} | 1×10^4 kN×m/rad | 1.05×10^4 kN×m/rad | 5.0% |

Table 7. As presented in Table 7, the bilinear stiffness values of the translational spring k_1 and k_2 , and the transitional load and displacement F_b and D_b are all well identified. The maximum error of the identified boundary parameter of the translational spring is within 2%. The bilinear stiffness values of the rotational spring k_{r1} and k_{r2} , and the transitional moment M_b and rotational angle θ_b are also well identified, and the error is within 9%.

3.3 Dead load effect on boundary parameter identification of a beam structure with bilinear boundary conditions

A real structure is not only subjected to temperature load, but also dead load and live load. It is likely that boundary conditions of the structure will enter into the nonlinear stage due to the combined action of temperature load, dead load and live load. Especially, when the strain gauges are installed in the structure before it begins to bear the dead load, the measured strain includes the strain caused by the dead load. Since the temperature load varies much slower than the vehicle load varies, therefore, the fast varying portion of the strain induced by the vehicle live load can be simply filtering out. Therefore, in this section, the vehicle live load is not considered in this section. However, the dead load, especially when the structure is forced assembly, may causes significant assembly stress of the bearing, and the bearing that contains assembly stress may be more easily to enter the nonlinear stage due to temperature load.

In this case, a beam structure as shown in Fig. 10 is considered. The strain sensors are assumed installed at the bottom of 1/10-span, 2/10-span, ..., and 10/10-span. The basic parameters of the beams structure are also presented in Table 1. The constitutive relation curve between force and displacement is presented in Fig.11. The real stiffness values of the bilinear translational spring are, $k_1=100$ kN/mm, $k_2=30$ kN/mm, the real transitional load is, $F_b=420$ kN, the real transitional displacement is, $D_b=4.2$ mm. The real stiffness values of the linear rotational spring is $k_r=1 \times 10^4$ kN×m/rad. In this case, we considered the translational spring transfer to the second nonlinear stage when the bearing load reaches to 420 kN. In real case, the translational spring is probably hard to enter the nonlinear range only due to temperature load. However, with the

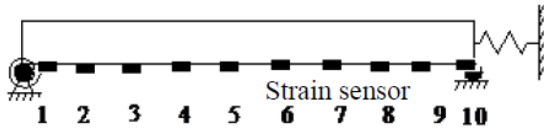


Fig. 10 The simulated beam structure with bilinear translational spring and rotational spring at each end considering dead load effect

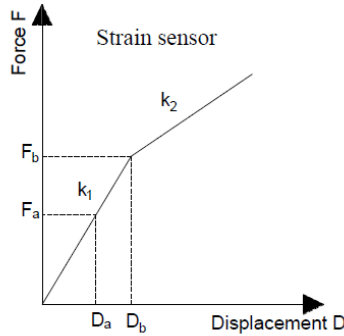


Fig. 11 The constitutive relationship of the force-displacement curve of the bilinear translational spring subjected to the dead load and temperature load

Table 8 Temperature load cases

| Temperature load case | The increased temperature on the top surface (°C) | The increased temperature on the bottom surface (°C) |
|-----------------------|---|--|
| 1 | 89.5 kN | 90.5 KN |
| 2 | 0.9 mm | 0.89 mm |
| 3 | 100 kN/mm | 101 kN/mm |
| 4 | 30 kN/mm | 30.7 kN/mm |

combination with the dead load and live load, the spring may enter the nonlinear stage. In this case, the rotational spring is considered as a linear spring, since the dead load induces opposite sign strain of the temperature induced strain, which will not let the rotational spring enter into the nonlinear stage. In this case, the dead load F_a is set to 100 kN/m. The temperatures of top surface and bottom surface are both assumed to be increased. The six temperature load cases are presented in Table 8.

The measured strains including dead load effect of the measured points are presented in Fig. 12. The strains induced by dead load are presented in Fig. 13. It is necessary to eliminate strain of beam structure caused by dead load, and then identify parameters of the boundary condition of the beam structure by using the proposed method based on the temperature effect. Usually, the strain due to dead load can be obtained when the structure is just constructed without bearing any load. In our case, the simulated strains due to dead load are directly subtracting from the total strain. The strains due to temperature loads are presented in Fig. 14.

An objective function as same as Eq. (9) can be created based on the temperature induced strains. The nonlinear least squares optimization algorithm is also used to optimize the objective function. The identified boundary parameters

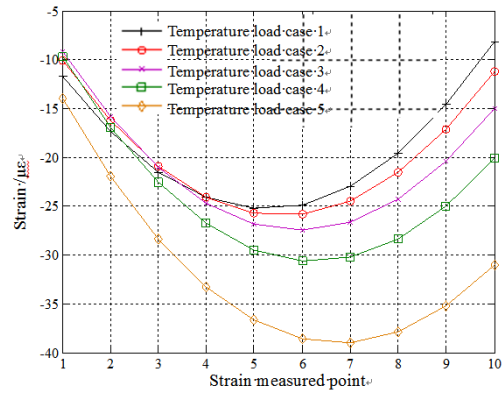


Fig. 12 Strain data of measure points due to dead load and temperature load

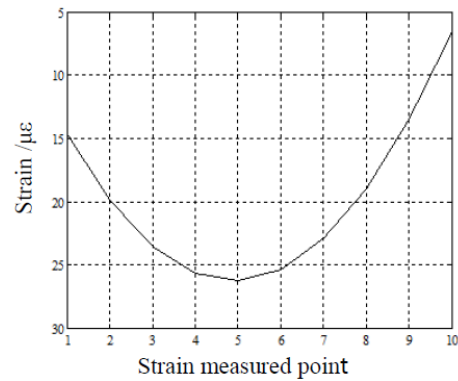


Fig. 13 Strain data due to dead load

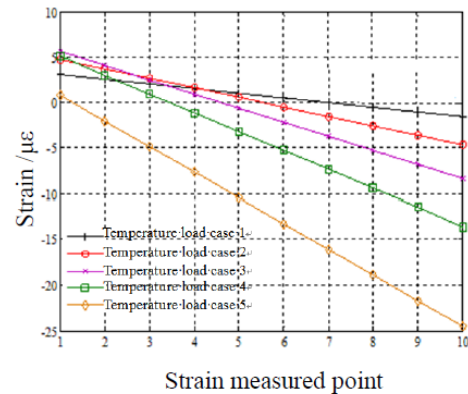


Fig. 14 Strain data due to temperature load cases

of the beam structure are illustrated in Table 9. As presented in Table 9, the boundary parameters are effectively identified based on the proposed method.

4. Boundary parameter identification of Yuanze bridge

In this section, based on the Yuanze bridge’s measured strain data, the proposed method is used to identify the boundary parameters of the bridge finite element model. Then, the temperature induced responses of the bridge are recalculated.

Table 9 The identified boundary parameters of a beam structure considering dead load effect

| The identified parameter | Theoretical value | Identified value | error |
|--------------------------|--|---|-------|
| F_b | 420 kN | 411 kN | -2% |
| D_b | 4.20 mm | 4.11 mm | -2% |
| k_1 | 100 kN/mm | 100 kN/mm | 0% |
| k_2 | 30 kN/mm | 31.5 kN/mm | 5% |
| k_r | $1 \times 10^4 \text{ kN} \times \text{m/rad}$ | $1.04 \times 10^4 \text{ kN} \times \text{m/rad}$ | 4% |

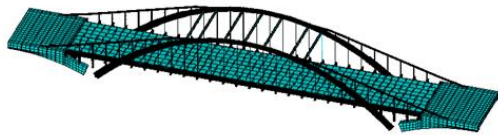


Fig. 15 The finite element model of Yuanze bridge



Fig. 16 Strain gauges layouts

4.1 The bridge background and the finite element model establishment

Yuanze bridge is an important bridge across Qingyi river, in Wuhu city, Anhui province in China. The main bridge is a mid-height deck steel pipe concrete tied arch bridge with auxiliary arches. The span arrangement of the bridge is 40 m+135 m+40 m. Based on the design and construction plan, the three-dimensional finite element model of the bridge is established. The initial bridge finite element model, with pinned boundary conditions, is shown in Fig. 15. The finite element model contains 1340 beam188 elements, 432 shell63 elements, 38 link10 elements, 2016 solid45 elements and 495 mass21 elements.

4.2 Installation of sensors and data acquisition

Since two sliding rubber bearing are used in the bridge, therefore, two boundary parameters of the bridge are selected for identification. In order to identify the finite element boundary parameters of Yuanze bridge, two strain gauges are installed at the two ends of the bridge to measure the longitudinal strains (Fig. 16). Since the strain gauges are installed after the construction of the bridge, therefore, the measured strains are induced the strains induced by live load and temperature load. Strain data are acquired by using the strain gages. Since the temperature sensors and strain sensors are shared with same strain gauges, the temperature changes (the difference between the temperature when installed the strain gauges and the temperature when measure the data) of the bridge are also measured.

The strains at the two measured points during 24 hours are measured. The temperature changes are also measured. In this section, the temperature is assumed as uniformly change of the whole bridge. The average temperature of the two measure points in 24 hours are presented in Fig. 17.

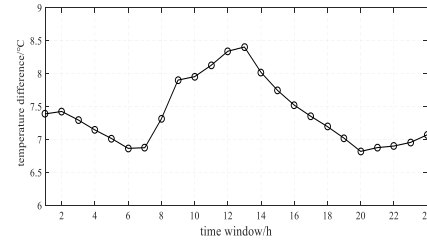
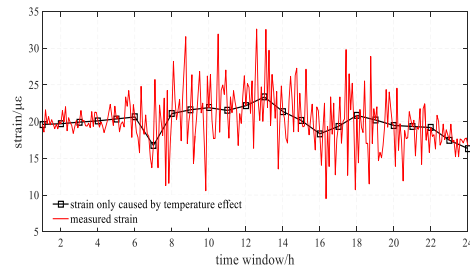
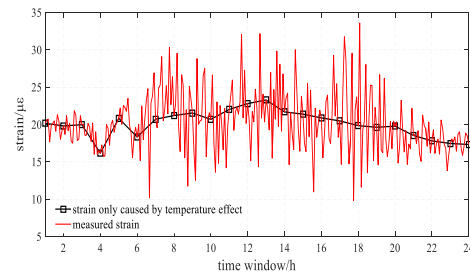


Fig. 17 The average temperature change of the two measured points



(a) The strain data at measured point 1 at the left end of the bridge

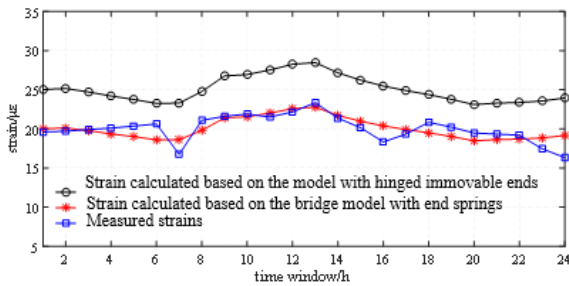


(b) The strain data at measured point 2 at the right end of the bridge

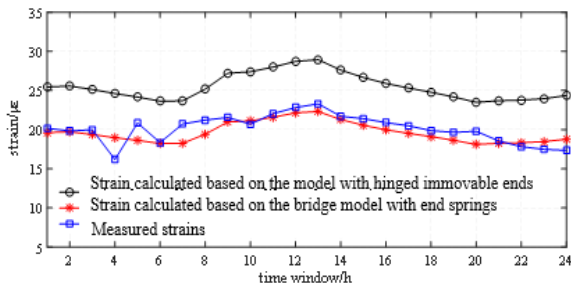
Fig. 18 The measured strain data of the bridge

The measured strain data are presented in Fig. 18. The red solid lines in Fig. 18 are the measured strain data with sampling rate of 0.2 measured data per minute. The measured strains including the vehicle load and temperature load effects. Since the temperature varies much slower than the vehicle load varies, therefore, the slow varying portion of the strain is induced by the temperature load. Therefore, the square dotted black lines are the slow varying strain by filtering from the original data. To further for the bridge model boundary parameter identification, every one hour temperature induced strains of each measured point are selected for the boundary parameters identification.

In order to further verify the accuracy of the bridge model, the temperature induced strains during due to the bridge model with hinged immovable supports (the boundary bearing are designed hinged immovable supports) and the bridge mode with translational springs are recalculated. The uniformly temperature changes as presented in Fig. 17 are considered for the simulation. The comparison of the simulated strains and the measured strains are presented in Fig. 19. As presented in Fig. 19, the recalculated strains based on the bridge finite element model with spring ends are in a good agreement with the measure data.



(a) The recalculated strains and measured strains at measured point 1 due to temperature load of Yuanze bridge



(b) The recalculated strains and measured strains at measured points due to temperature load of Yuanze bridge

Fig. 19 The recalculated strains and measured strain

Table 10 The identified boundary parameter

| | Identified results (kN/mm) |
|-------------------------|----------------------------|
| Left end of the bridge | 936.5 |
| Right end of the bridge | 943.6 |

4.3 Boundary parameter identification of Yuanze bridge

To obtain the boundary parameter of the bridge, the boundary conditions of the two ends of the bridge are simulated as translational spring. Again, the temperature induced strains (measured every one hour) of each measured point are selected for the boundary parameters identification. Since the bearings of the real bridge do not perform nonlinear behavior, only the linear boundary parameters of the springs are identified. On the basis of the temperature induced strains, the optimization objective function shown can be created based on the propose method. The boundary parameters are identified by nonlinear least squares optimization algorithm. Table 10 illustrates final identified linear boundary parameters of the bridge model.

5. Conclusions

In this paper, the nonlinear boundary conditions of the bridge model are identified based on the measured temperature-induced responses. The temperature-induced responses of a simply support beam with nonlinear translational and rotational boundary conditions subjected to various temperature loads are analyzed. The objective function based on the temperature-induced responses is

created, and the nonlinear boundary conditions can be identified by using the nonlinear least squares optimization algorithm. A beam structure with nonlinear translational and rotational springs is simulated as a numerical example, and the nonlinear boundary parameters of the model are identified based on the proposed method. The boundary parameters of a real arch bridge are also identified based on the propose method. Based on the theoretical derivations, numerical simulations, and the real bridge application, the specific conclusions of this paper can be summarized below.

- For a beam structure, the translational boundary condition of the structure indicates proportionally to temperature effect caused by uniform temperature change, and rotational boundary condition also present proportionally to temperature gradients. Based on the relation between the temperature induced responses and boundary conditions, the boundary parameters can be identified using the optimization method.

- Through the numerical simulation of a beam structure with nonlinear translational and rotational boundary conditions, the nonlinear boundary parameter can be effectively identified based on the temperature induce responses. The temperature induced strain can also be easily extracted from the measure strains including the strains due to dead and live loads.

- On the basis of temperature induced strains, the boundary parameters of Yuanze bridge model are identified. Based on the bridge model with spring ends, the temperature induced strains are recalculated. The recalculated strains based on the bridge model with spring ends are in a good agreement with the measure data.

Acknowledgments

Financial support to complete this study was provided in part by the National Natural Science Foundation of China under grand No. 51578206, by the Natural Science Funds for Distinguished Young Scholar of Anhui province under grand No.1708085J06, by the key research and development project of Anhui province under grand No. 1804a0802204, and by the Fundamental Research Funds for the Central Universities under grand No. PA2017GDQT0022. The results and opinions expressed in this paper are those of the authors only and they don't necessarily represent those of the sponsors.

References

- Alamdari, M.M., Li, J.C., Samali, B., Ahmadian, H. and Naghavi, A. (2014), "Nonlinear joint model updating in assembled structures", *J. Eng. Mech. ASCE*, **140**(7), 04014042.
- Brownjohn, J.M.W., Xu, Y.L. and De, S. (2011), "Vibration-based monitoring of civil infrastructure: Challenges and successes", *J. Civil Struct. Health. Monit.*, **1**(3), 79-95.
- Chaudhary, M.T.A., Abe, M. and Fujino, Y. (2002), "Role of structural details in altering the expected seismic responses of base-isolated bridges", *Mech. Syst. Sign. P.R.*, **16**(2-3), 413-428.
- Chen, Z.W., Zhu, S.Y., Xu, Y.L., Li, Q. and Cai, Q.L. (2015), "Damage detection in long suspension bridges using stress

- influence lines”, *J. Brid. Eng. ASCE*, **20**(3), 1-11.
- Dai, W., Moroni, M.O., Roesset, J.M. and Sarrazion, M. (2006), “Effect of isolation pads and their stiffness on the dynamic characteristics of bridges”, *Eng. Struct.*, **28**(9), 1298-1306.
- Deng, Y., Ding, Y.L. and Li, A.Q. (2010), “Structural condition assessment of long-span suspension bridges using long-term monitoring data”, *Earthq. Eng. Eng. Vibr.*, **9**(1), 123-131.
- Dilger, W.H., Amin, G., Chan, M., Mo, S.C. and Maes, M.A. (1983), “Temperature stress in composite box girder bridges”, *J. Struct. Eng. ASCE*, **109**(6), 1460-1479.
- Ding, Y., Wang, G., Zhou, G. and Li, A. (2013), “Life-cycle simulation method of temperature field of steel box girder for Runyang cable-stayed bridge based on field monitoring data”, *Chin. Civil Eng. J.*, **46**(5), 129-136.
- Gao, K., Yuan, W.C. and Dang, X.Z. (2017), “Development and experimental study on cable-sliding modular expansion joints”, *Struct. Eng. Mech.*, **61**(6), 795-806.
- He, X., Moaveni, B., Conte, J., Elgamal, A. and Masri, S.F. (2009), “System identification of Irfed Zampa Memorial bridge using dynamic field test data”, *J. Struct. Eng. ASCE*, **135**(1), 54-66.
- Jaishi, B. and Ren, W.X. (2005), “Structural finite element model updating using ambient vibration test results”, *J. Struct. Eng. ASCE*, **131**(4), 617-628.
- Kennedy, J.B. and Soliman, M.H. (1987), “Temperature distribution in composite bridges”, *J. Struct. Eng. ASCE*, **113**(3), 475-482.
- Lei, Y., Hua, W., Luo S.J. and He M.Y. (2015), “Detection and parametric identification of structural nonlinear restoring forces from partial measurements of structural responses”, *Struct. Eng. Mech.*, **54**(2), 291-304.
- Li, J., Hao, H., Xia, Y. and Zhu, H.P. (2015), “Damage assessment of shear connectors with vibration measurements and power spectral density transmissibility”, *Struct. Eng. Mech.*, **54**(2), 257-289.
- Marquardt, D.(1963), “An algorithm for least-squares estimation of nonlinear parameters”, *SIAM J. Appl. Math.*, **11**(2), 431-441.
- Moaveni, B. and Behmanesh, I. (2012), “Effects of changing ambient temperature on finite element model updating of the dowling hall footbridge”, *Eng. Struct.*, **43**(10), 58-68.
- Nagayama, T., Abe, M., Fujino, Y. and Ikeda, K. (2005), “Structural identification of a non-proportionally damped System and its application to a full-scale suspension bridge”, *J. Struct. Eng. ASCE*, **131**(10), 1536-1545.
- Ni, Y.Q., Hua, X.G., Wong, K.Y. and Ko, J.M. (2007), “Assessment of bridge expansion joints using long-term displacement and temperature measurement”, *J. Perform. Constr. Facil.*, **21**(2), 143-151.
- Ren, W.X., Peng, X.L. and Lin, Y.Q. (2005), “Experimental and analytical studies on dynamic characteristics of a large span cable-stayed bridges”, *Eng. Struct.*, **27**(4), 535-548.
- Roberts-Wollman, C.L., Breen, J.E. and Cawrse, J. (2002), “Measurements of thermal gradients and their effects on segmental concrete bridge”, *J. Brid. Eng. ASCE*, **7**(3), 166-174.
- Shahawy, M.A. and Arockiasamy, M. (1996), “Analytical and measured strains in sunshine skyway bridge II”, *J. Brid. Eng. ASCE*, **1**(2), 87-97.
- Tong, M., Tham, L.G., Au, F.T.K. and Lee, P.K.K. (2001), “Numerical modelling for temperature distribution in steel bridges”, *Comput. Struct.*, **79**(6), 583-593.
- Wang, Z.C., Geng, D., Ren, W.X., Chen, G.D. and Zhang, G.F. (2015), “Damage detection of nonlinear structures with analytical mode decomposition and hilbert transform”, *Smart Struct. Syst.*, **15**(1), 1-13.
- Wang, Z.C., Xin, Y. and Ren, W.X. (2016), “Nonlinear structural joint model updating based on instantaneous characteristics of dynamic responses”, *Mech. Syst. Sign. P.R.*, **76**, 476-496.
- Wei, J.J. and Lv, Z.R. (2015), “Structural damage detection including the temperature difference based on response sensitivity analysis”, *Struct. Eng. Mech.*, **53**(2), 249-260.
- Xia, Y., Xu, Y.L., Wei, Z.L., Zhu, H.P. and Zhou, X.Q. (2011), “Variation of structural vibration characteristics versus non-uniform temperature distribution”, *Eng. Struct.*, **33**(1), 146-153.
- Xu, Y.L., Chen, B., Ng, C.L., Wong, K.Y. and Chan, W.Y. (2009), “Monitoring temperature effect on a long suspension bridge”, *Struct. Contr. Health Monit.*, **17**(6), 632-653.
- Yang, X., Zhang, J. and Ren, W.X. (2017), “Temperature effect analysis of a long-span cable-stayed bridge based on extreme strain estimation”, *Smart Struct. Syst.*, **20**(1), 11-22.
- Yarnold, M.T. and Moon, F.L. (2015), “Temperature-based structural health monitoring baseline for long-span bridge”, *Eng. Struct.*, **86**, 157-167.
- Yarnold, M.T., Moon, F.L. and Aktan, A.E. (2015), “Temperature-based structural identification of long-span bridges”, *J. Struct. Eng. ASCE*, **141**(11), 1-10.
- Yu, L. and Zhu, J.H. (2015), “Nonlinear damage detection using higher statistical moments of structural responses”, *Struct. Eng. Mech.*, **54**(2), 221-237.
- Zhang, J. and Prader, J. (2013), “Experimental vibration analysis for structural identification of a long-span suspension bridge”, *J. Eng. Mech. ASCE*, **139**(6), 748-759.

CC